The accuracy of membrane potential reconstruction based on spiking receptive fields

Deepankar Mohanty, Benjamin Scholl and Nicholas J. Priebe

J Neurophysiol 107:2143-2153, 2012. First published 25 January 2012; doi:10.1152/jn.01176.2011

Journal of Neurophysiology publishes original articles on the function of the nervous system. It is published 12 times a year (monthly) by the American Physiological Society, 9650 Rockville Pike, Bethesda MD 20814-3991. ISSN: 0022-3077, ESSN: 1522-1598. Visit our website at http://www.the-aps.org/.

J Neurophysiol 107: 2143–2153, 2012.
First published January 25, 2011; doi:10.1152/jn.01176.2011.

The accuracy of membrane potential reconstruction based on spiking receptive fields

Deepankar Mohanty, Benjamin Scholl, and Nicholas J. Priebe
Center for Perceptual Systems, Section of Neurobiology, School of Biological Sciences, College of Natural Sciences, The University of Texas at Austin, Austin, Texas

Submitted 21 December 2011; accepted in final form 20 January 2012

Mohanty D, Scholl B, Priebe NJ. The accuracy of membrane potential reconstruction based on spiking receptive fields. *J Neurophysiol* 107: 2143–2153, 2012. First published January 25, 2011; doi:10.1152/jn.01176.2011.—A common technique used to study the response selectivity of neurons is to measure the relationship between sensory stimulation and action potential responses. Action potentials, however, are only indirectly related to the synaptic inputs that determine the underlying, subthreshold, response selectivity. We present a method to predict membrane potential, the measurable result of the convergence of synaptic inputs, based on spike rate alone and then test its utility by comparing predictions to actual membrane potential recordings from simple cells in primary visual cortex. Using a noise stimulus, we found that spike rate receptive fields were in precise correspondence with membrane potential receptive fields ($R^2 = 0.74$). On average, spike rate alone could predict 44% of membrane potential fluctuations to dynamic noise stimuli, demonstrating the utility of this method to extract estimates of subthreshold responses. We also found that the nonlinear relationship between membrane potential and spike rate could also be extracted from spike rate data alone by comparing predictions from the noise stimulus with the actual spike rate. Our analysis reveals that linear receptive field models extracted from noise stimuli accurately reflect the underlying membrane potential selectivity and thus represent a method to generate estimates of the underlying average membrane potential from spike rate data alone.

primary visual cortex; spike threshold; intracellular recording; simple cells

THE PRIMARY MODE OF COMMUNICATION between neurons in cortex is synaptic transmission triggered by action potentials. Action potentials, or spikes, result when a neuron's many synaptic inputs combine to cause it to reach a critical membrane potential threshold. Whereas a neuron's spiking response to a sensory stimulus defines the information it is communicating to downstream neurons, the selectivity of its response is determined by the convergence of its synaptic inputs via upstream neurons. Understanding the basis for sensory selectivity, therefore, requires knowledge of the selectivity of the afferent synaptic inputs.

We know that the aggregate synaptic input, and therefore the response selectivity of such input, to a neuron is represented by its membrane potential fluctuations in response to sensory stimulation; however, direct measurement of membrane potential requires intracellular recordings, which are difficult to obtain relative to extracellular (spiking) recordings. Therefore, a method of estimating the underlying membrane potential selectivity from extracellular recordings of spikes alone would be important for providing visibility into the selectivity of synaptic inputs in cortex.

Such estimation, however, has historically been challenged by the presence of the intervening action potential threshold. Threshold acts as a filter for the neuron: stimuli that do not evoke a sufficient depolarization for the neuron to reach threshold do not generate spikes, and as such, the effectiveness of these stimuli is overlooked. This filtering action of threshold is evident in several experimental models of cortex. For example, in primary visual cortex (V1), neuronal spike rate selectivity is higher than membrane potential selectivity for orientation (Carandini and Ferster 2000; Monier et al. 2003), direction (Jagadeesh et al. 1997; Priebe and Ferster 2005), and spatial receptive fields (Bringuier et al. 1999). In auditory (Tan et al. 2004) and barrel cortex (Moore and Nelson 1998), spike rate selectivity is also increased relative to membrane potential selectivity. This intervening threshold nonlinearity, while critical to cortical response selectivity, has precluded the translation of physiologically measured spiking responses into their underlying membrane potential responses and, in turn, the important characterization of the underlying synaptic inputs.

We demonstrate here that it is indeed possible to recover membrane potential selectivity from recorded spiking selectivity alone, using a dynamic noise stimulus. With the use of a dynamic noise stimulus, spike rate receptive field estimates should not be distorted by the threshold nonlinearity, and their membrane potential and spike rate selectivities, as represented by their receptive fields, should be the same (Chichilnisky 2001; Simoncelli et al. 2004).

We used intracellular recordings, which allow access to both the suprathreshold spike rate and subthreshold membrane potential, to determine how our receptive fields based on spike rate compare with membrane potential receptive fields. Receptive fields of V1 simple cells are virtually identical for membrane potential and spike rate. Furthermore, the average membrane potential time course can be accurately predicted from spike rate receptive fields. Finally, we demonstrate that the nonlinear relationship between recorded membrane potential and spike rate may be accurately estimated from our spike rate measures. Overall, we found that this technique provides an accurate prediction of the average underlying membrane potential solely on the basis of the spiking responses, demonstrating that it is possible to estimate subthreshold selectivity solely on the basis of suprathreshold responses for simple cells in V1.

METHODS

Physiological recordings and visual stimulation. Whole cell patch-clamp recordings were made in vivo from neurons in V1 in anesthe-

Address for reprint requests and other correspondence: N. J. Priebe, Section of Neurobiology, The Univ. of Texas at Austin, 2400 Speedway, Austin, TX 78705 (e-mail: nicholas@mail.utexas.edu).

tized, paralyzed cats (2–2.5 kg) as has previously been described (Priebe and Ferster 2005). Anesthesia was induced with ketamine (5–15 mg/kg) and acepromazine (0.7 mg/kg) and followed by intravenous (IV) administration of thiopental sodium (10–20 mg/kg) during surgery. After surgery, the animal was placed in the stereotaxic frame until the end of the experiment. Recording stability was increased by both suspending the thoracic vertebrae from the stereotaxic frame and performing a pneumothoracotomy. Eye drift was minimized with the IV infusion of vecuronium bromide (Norcuron, 0.2 $mg\cdot^{-1}kg\cdot h^{-1}$). Anesthesia was maintained for the duration of the experiment with the continuous infusion of thiopental sodium (Hospira, 1–3 $mg\cdot^{-1}kg\cdot h^{-1}$). Body temperature, ECG, EEG, CO_2, and autonomic signs were continuously monitored. The nictitating membrane was retracted using phenylephrine hydrochloride, and the pupils were dilated using topical atropine. Contact lenses with artificial pupils were inserted to protect the corneas. Supplementary lenses were selected by direct ophthalmoscopy to focus the display screen onto the retina.

Borosilicate glass electrodes (A-M Systems, Carlsborg, WA) were filled with a K-gluconate-based solution (in mM: 130 K-gluconate, 2 $MgCl_2$, 0.5 EGTA, 10 HEPES, 2 Mg-ATP, 2 Na-GTP, 20 Tris-phosphocreatine). After a craniotomy was made above area 17 (~2 mm lateral of the midline), a small hole in the dura was made and an electrode was advanced into the cortex with a motorized microdrive (Sutter Instruments, Novato, CA). After the electrode was in place, warm agarose solution (3% in normal saline) was placed over the craniotomy to protect the surface of the cortex and reduce pulsations. All procedures were approved by The University of Texas at Austin Institutional Animal Care and Use Committee.

Visual stimuli were generated by a Macintosh computer (Apple, Cupertino, CA) using the Psychophysics Toolbox (Brainard 1997; Pelli 1997) for Matlab (The MathWorks, Natick, MA) and presented on a Sony GDM-F520 video monitor placed 50 cm from the animal's eyes. The video monitor had a noninterlaced refresh rate of either 100 or 120 Hz and a spatial resolution of at least 1,280 × 1,024 pixels, which subtended 38 cm horizontally and 30 cm vertically. The video monitor had a mean luminance of 45 cd/m^2.

Noise stimuli were presented for between 8 and 20 s and were preceded and followed by at least 250-ms blank (mean luminance) periods. For each recorded V1 neuron, after its preference was initially characterized for orientation, spatial frequency, spatial location, and stimulus size for each eye, a one-dimensional noise stimulus at the preferred orientation was presented to the preferred eye (Citron and Emerson 1983; Mclean and Palmer 1988; Priebe and Ferster 2005). At each location the luminance was light, gray, or dark with probabilities 0.25, 0.5, and 0.25, respectively. Voltage responses were sampled at 4,096 Hz and stored for subsequent analysis. A new noise stimulus was presented at the frame rate of the monitor. The temporal sequence of bars in each trial was controlled by setting an initial random seed, which could either vary or be fixed across trials. Receptive field estimates were based on trials collected in which the random seed varied. Validation of receptive fields was accomplished by comparing the response to the trials in which the random seed was fixed with the predicted response based on the receptive field. All of the neurons reported here had a spiking modulation ratio (F1/F0) at the preferred spatial frequency >1 and were therefore classified as simple cells (Skottun et al. 1991).

Analysis. Spikes were identified from the large characteristic deflections in membrane potential. Membrane potential was passed through a 5-ms median filter to remove the action potentials. Membrane potential and spike rate were then binned at the frame rate of the stimulus, either 100 or 120 Hz. Further analyses are described where appropriate in the RESULTS.

RESULTS

Comparing membrane potential and spike rate selectivity in a simple model. The central aim of this work was to demonstrate the degree to which membrane potential fluctuations in response to visual stimuli and selectivity may be accurately predicted by spike rate. To date, discrepancies in selectivity for membrane potential and spike rate, combined with the feasibility challenges of measuring membrane potential directly in vivo, have precluded visibility into the synaptic basis for response selectivity in cortical neurons. As such, the ability to map membrane potential from spiking data alone will have far-reaching utility across studies of cortical function.

The discrepancies in selectivity for membrane potential versus spike rate stem from experiments in which each stimulus condition is presented individually and the average response following the stimulus is measured. To demonstrate why this is the case, we constructed a model V1 neuron that depolarizes in response to a light bar flashed in either of two locations, but to a greater degree to *location 1* than to *location 2*. When plotted based on stimulus location (Fig. 1*A*), the selectivity of the model neuron is represented by a vector that leans closer to the ordinate than the abscissa, indicating that the neuron prefers a light bar presented in *location 1* versus *location 2*. Using this model neuron, we can now evaluate two different methods to estimate both spike rate and membrane potential selectivity, the first of which produces discrepant results.

The first method to characterize neuronal response selectivity is to measure the neuronal response to stimulation of each spatial location individually. This stimulus protocol is diagramed in Fig. 1*A*. Light bars flashed in each location separately are represented by two filled circles, one on the ordinate and one on the abscissa. The response of the model neuron is determined by drawing a projection from the stimulus (filled circle) onto the model neuron's selectivity vector. Because of the neuronal threshold nonlinearity, spikes are only elicited in response to the stimulus flashed at *location 1* (Fig. 1*A*, red) and not at *location 2* (Fig. 1*A*, blue), yet membrane potential depolarizations are elicited in response to the stimulus at both locations. Therefore, the selectivity of the model neuron differs substantially when measured via depolarizations versus spike rate. This is evident in Fig. 1*A*, *inset*, in which the vectors representing spike rate selectivity and membrane potential selectivity point in different directions.

An alternative method to characterize neuronal response selectivity is to use a noise stimulus that samples the visual space of stimulus conditions more broadly (see also Chichilnisky 2001 and Simoncelli et al. 2004 for descriptions of this method). To do so, the luminance of the bars is randomly varied using a Gaussian distribution and simultaneously displayed at each bar location (Fig. 1*B*). As when we presented the bars individually (Fig. 1*A*), the response to each stimulus condition is determined by the projection onto the selectivity vector and is indicated by color (Fig. 1*B*). Importantly, the stimulus distribution is Gaussian, and therefore the threshold nonlinearity will not distort the spike rate selectivity and membrane potential selectivity as we observed when the bars were presented individually. That is, the subthreshold response to both bars will be revealed in spike rate, since in this stimulus method, the simultaneous presentation of bars at both locations

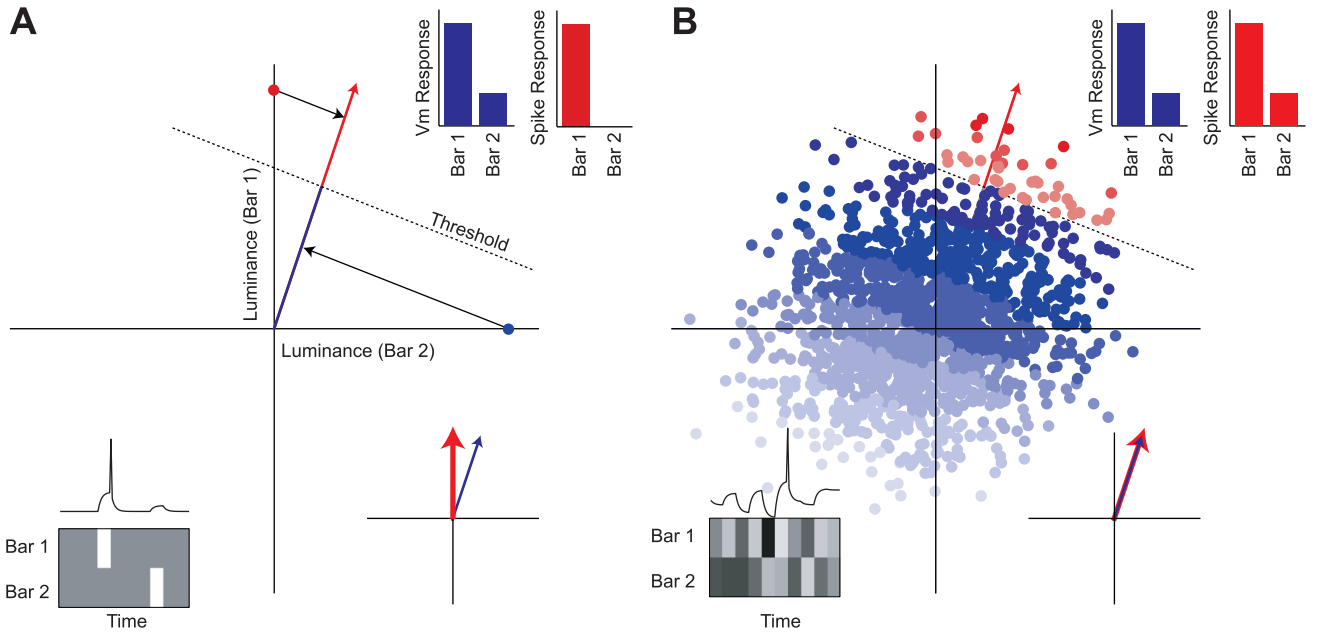

Fig. 1. A simple model of the visual responses to bars of light. A model neuron with a spike threshold responds to light in 2 locations but depolarizes more to *location 1* than *location 2*. *A*: the paradigm in a typical electrophysiology experiment is to present each stimulus alone and measure the response to that stimulus. Each stimulus is indicated by a filled circle, and the model response is indicated by color (blue, subthreshold; red, suprathreshold). The receptive field of the neuron is represented by the vector tilted toward the ordinate, indicating a preference for light presented in *location 1*. The response to each stimulus is computed by drawing the projection of the stimulus onto the vector representing the receptive field (arrows). Threshold is represented by a line orthogonal to the receptive field. Because the light bar presented at *location 1* alone projects onto the receptive field above threshold, this stimulus evokes neuronal spiking, whereas the light bar presented at *location 2* alone depolarizes the model neuron but does not cause it to reach threshold for spiking (example trace at *bottom*). The average subthreshold and suprathreshold responses are indicated by bar graphs (*inset*). *B*: same conventions as in *A* but using a noise stimulus in which light bars may be presented in both *locations 1* and *2* simultaneously. V_m, membrane potential.

uncovers the depolarizing effect of light in *location 2*. Although a light bar in *location 2* on its own does not elicit a suprathreshold response, increasing luminance in *location 2* has the effect of lowering the amount of light required in *location 1* to elicit a suprathreshold response. Thus the measured spike rate selectivity of the model neuron is not altered by the intervening threshold nonlinearity and matches the underlying membrane potential selectivity, and the vectors characterizing selectivity based on this noise method point in the same direction. The spike rate selectivity based on the response to the noise stimulus faithfully represents the membrane potential selectivity.

There are two essential requirements for this alternative method of extracting membrane potential selectivity from spike rate selectivity (Chichilnisky 2001). First, this method requires that the projection of the stimulus onto the receptive field be radially symmetric. This may be accomplished by using a number of different noise distributions, but Gaussian noise distributions, such as the varied luminance stimulus we presented to the model neuron, generally fulfill this requirement. Second, the intervening nonlinearity between membrane potential and spike rate must be static. That is, the threshold level cannot change as a function of the stimulus parameters.

Comparing membrane potential and spike rate selectivity in V1 simple cells. To assess whether the alternative method we describe can be used to extract membrane potential selectivity from spike rate, we made intracellular recordings from simple cells in cat V1 in vivo. Our intracellular records, from which both sub- and suprathreshold responses are available, allow us to test the degree to which spike rate selectivity matches membrane potential selectivity. We initially characterized each recorded neuron by measuring selectivity for orientation, spatial frequency, ocular dominance, and receptive field size. Stimulus bars of the preferred orientation were then presented in a pseudorandom sequence over the appropriate receptive field. Each bar was presented as dark, light, or gray, and these luminance values were updated at the frame rate of the visual display (Fig. 2*A*). Intracellular records were split into two separate components, one corresponding to spike rate and the other to the underlying membrane potential with the action potentials removed by median-filtering the data (Fig. 2*A*) (Jagadeesh et al. 1997). Linear filters, or receptive fields, were generated by computing the cross-correlation of the spike rate or the membrane potential and the noise stimulus (Fig. 2*A*) (Anzai et al. 1999; Dayan and Abbott 2001; Rieke et al. 1997).

As is characteristic of V1 simple cells, our recorded neurons displayed a preference for dark and light stimuli in distinct nonoverlapping locations of the visual field after a visual latency (Fig. 2*B*) (Hirsch et al. 1998; Hubel and Wiesel 1962; Skottun et al. 1991). The example neuron in Fig. 2 is selective for stimulus direction, as can be seen by the characteristic tilt in the spiking receptive field, indicating that its preference for bar location in the visual field changes over time (Reid et al. 1991). Receptive field maps based on membrane potential and spike rate were strikingly similar across the population of recorded neurons. For the example neuron in Fig. 2, the cross-correlation (R^2) between the two maps is 0.796, a value typical across our population of recorded simple cells (mean = 0.74 ± 0.12, n = 25). Therefore, the underlying membrane potential selectivity, as represented by the receptive field map, is accurately represented by spike rate selectivity.

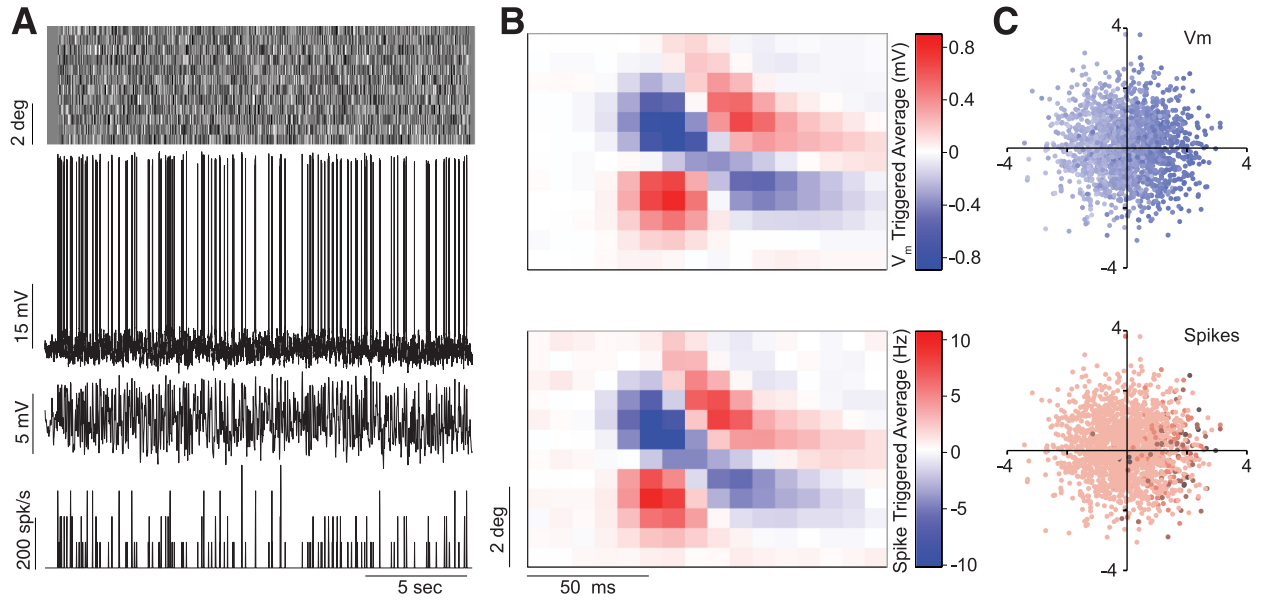

Fig. 2. Responses of a simple cell to noise stimulus. *A*: the noise stimulus consisted of bars at the preferred orientation that switched from light, gray, and dark (*top* row). The raw recorded membrane potential response to that noise sequence is plotted (2nd row). Membrane potential was separated from spikes by using a median filter to remove the large deviations in potential and resampled at the frame rate of the monitor (3rd row). Spike rate was extracted from the raw membrane potential trace and resampled at the frame rate of the monitor (*bottom* row). *B*: the linear membrane potential receptive field (*top*) and spike rate receptive field (*bottom*) extracted from records such as those shown in *A*. *C*: a low-dimensional representation of the stimulus. The projection of the stimulus onto the linear spiking receptive field is plotted on the abscissa and that onto an orthogonal receptive field is plotted on the ordinate. Each point indicates a single time point. Response is indicated by the intensity of each point: increases in membrane potential by dark blue (*top*) and increases in spike rate by dark red (*bottom*).

The stimulus-response relationship for membrane potential and spike rate may also be plotted using a two-dimensional representation, as in Fig. 1. Because our actual stimulus has more than the two dimensions of the example stimulus in Fig. 1, we plotted the projection of the actual stimulus (Fig. 2*A*) onto the membrane potential receptive field (Fig. 2*B*) to define the abscissa and onto an orthogonal dimension for the ordinate. As the stimulus matches the receptive field, represented by positive values along the abscissa, depolarization is observed (Fig. 2*C*, *top*) as well as increased spike rate (Fig. 2*C*, *bottom*).

Across the population of simple cells we found this striking similarity between membrane potential and spike rate receptive fields (6 additional examples in Fig. 3). This similarity, however, stands in marked contrast to the well-described differences in orientation, size, and direction selectivities of V1 neurons based on membrane potential versus spike rate (Bringuier et al. 1999; Carandini and Ferster 2000; Jagadeesh et al. 1997). In each of those cases, selectivity characterized via stimulus gratings or bars is much broader for membrane potential than for spike rate, yet in our current study the spatiotemporal components of the receptive field are in precise correspondence for both. The similarity we document here results from the specific noise stimulus we have utilized and the analysis we have employed to characterize the receptive fields, as in the model neuron shown in Fig. 1. When using such a dynamic noise stimulus, a linear receptive field can be recovered despite the presence of the intervening static nonlinearity (threshold). Because the characteristics of our chosen dynamic noise stimulus are approximately Gaussian, the similarity of receptive field profiles suggests that any intervening nonlinearity, such as threshold, is also static. There are slight differences in the membrane potential and spike rate receptive field maps from our records, but the differences appear to result from the different amounts of data available in each record. Specifically, generation of the spiking maps relies on the presence of discrete action potentials during visual stimulation, whereas membrane potential fluctuations are consistently present in the neuron during visual stimulation, yielding far more data for inclusion in our model.

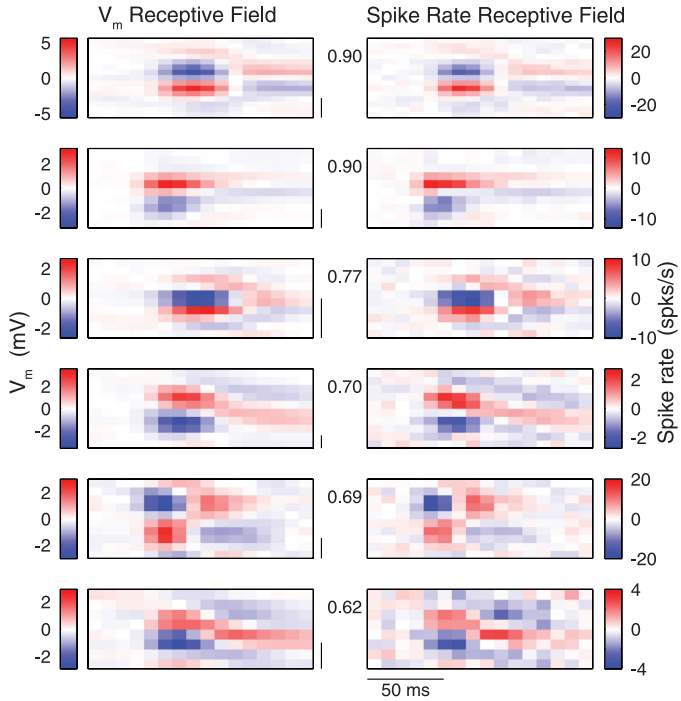

Fig. 3. Receptive field profiles for membrane potential and spike rate for simple cells. Membrane potential receptive fields (*left*) and spike rate receptive fields (*right*) are illustrated for 6 simple cells in V1. Each row shows the receptive fields for a single neuron. R^2 between the membrane potential and spike rate receptive fields is indicated by the number between the receptive field profiles. Neurons are sorted by the correlation between the 2 receptive fields. Scale bars indicate 1 degree.

Predicting membrane potential from recorded spikes. Given the similarity of membrane potential and spiking receptive fields elicited by the dynamic noise stimulus, we next asked how well membrane potential fluctuations could be predicted on the basis of the spiking receptive fields alone. We generated linear predictions of membrane potential response based on the spike rate receptive field and distinct noise stimulus sequences. Our predictions of membrane potential response are called generator potentials (e.g., GP_{SP} for the generator potential based on spiking). To compare the predicted membrane potential response (GP_{SP}) with our recorded membrane potential response, we normalized both by the standard deviation of each data set and measured their correlation (Ringach and Malone 2007). On average, the GP_{SP} accounted for only 17.3% of the membrane potential variance (R^2, $n = 25$).

Such poor performance may, however, be due to ongoing cortical activity that is responsible for trial-to-trial variability of recorded membrane potential responses. Our receptive field maps can only predict the average membrane potential response. To eliminate the effects of such variability and to enable appropriate comparisons, we measured and then averaged the membrane potential response to a single, specific noise sequence repeated many times (Fig. 4*A*, *top*). We then compared the GP_{SP} and the average membrane potential response across trials (Fig. 4*A*, *bottom*), which significantly improved the ability of the GP_{SP} to account for the recorded membrane potential, relative to the trial-by-trial comparison (from 15.2% to 38.9%, $n = 13$, $P < 0.05$; Fig. 5*A*).

Although trial averaging significantly reduced the impact of trial-to-trial noise, fluctuations in average response to the repeated sequence persisted because of the finite number of repeats in our data set. We therefore employed a method developed by Sahani and Linden (2003) to estimate the amount of variance that may be accounted for by our model, based on the degree of trial-by-trial fluctuation and the number of stimulus repeats. For this method, the response is assumed to be composed of two features, the signal component, μ, that exists on each trial and a noise component, η, that varies from trial to trial. The variance of the signal over the stimulus period, $\sigma^2(\mu)$, is defined as

$$\sigma^2(\mu) = \frac{1}{N-1}\left[N\sigma^2(\overline{r^{(n)}}) - \overline{\sigma^2(r^{(n)})}\right], \quad (1)$$

where N is the number of stimulus repeats, and $r^{(n)}$ is the membrane potential response to each stimulus presentation.

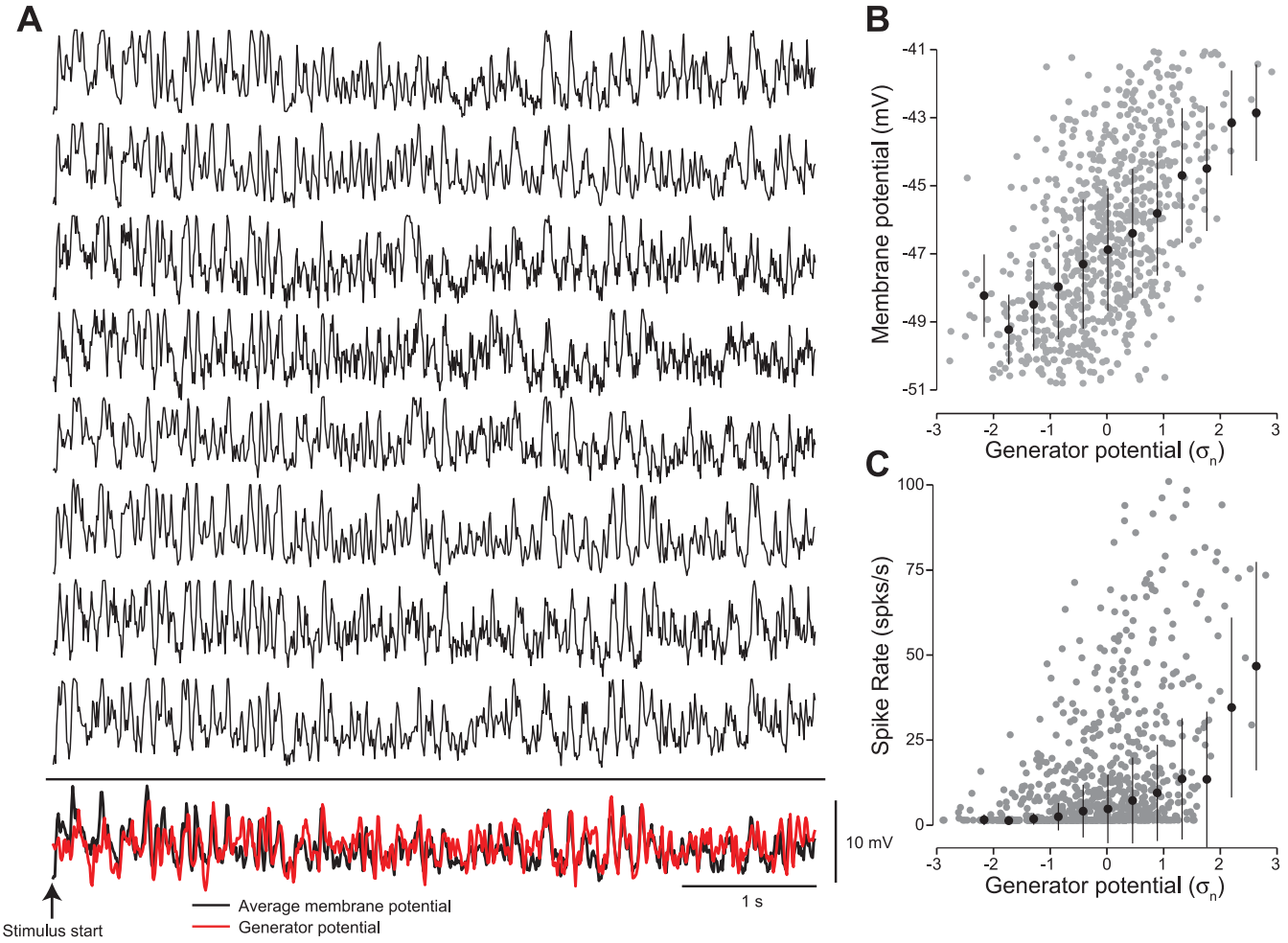

Fig. 4. Measuring responses to the same stimulus. *A*: responses of a neuron to 8 repeats of the same noise stimulus (*top*). Responses to that particular noise stimulus were averaged (*bottom*, black trace) and the generator potential based on spiking (GP_{SP}) derived (*bottom*, red trace). *B*: comparisons of recorded membrane potential and GP_{SP}. Each gray point indicates the GP_{SP}, normalized by the standard deviation of GP_{SP} (σ_n), and recorded membrane potential for a single frame of the stimulus. Black symbols and error bars indicate the average and standard deviation of the relationship. *C*: same conventions as in *B* but a comparison of recorded spike rate and GP_{SP}.

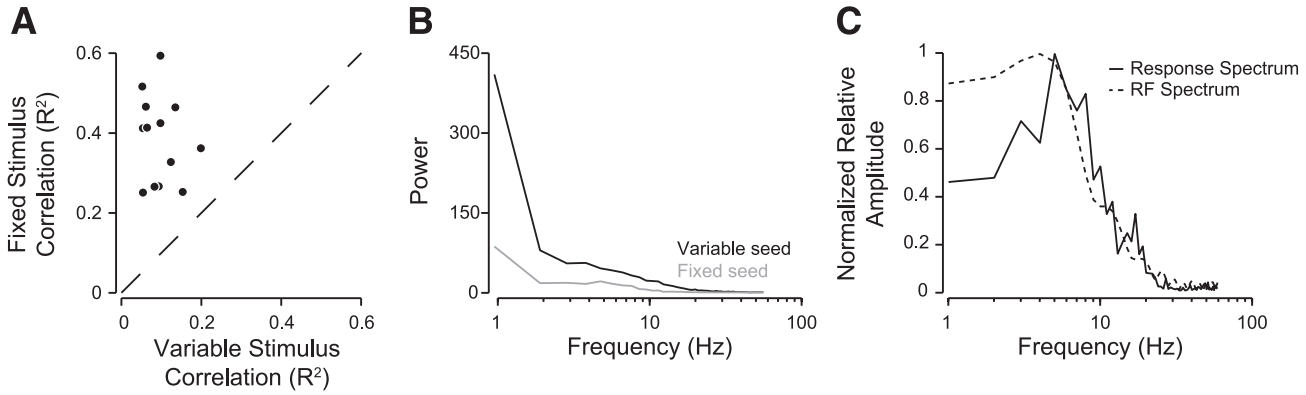

Fig. 5. Comparison of model accuracy using trial-to-trial or average membrane potential responses. *A*: each point indicates a different neuron in the sample population. Model predictions were significantly better for average responses than for trial-to-trial responses. *B*: average power spectrum of the response to the noise stimulus when it varied on a trial-to-trial basis (variable seed) is plotted with the power spectrum of the average response to the same noise stimulus (fixed seed). *C*: ratio of the 2 power spectra shown in *A* after having been normalized to the peak ratio (response spectrum). The power spectrum of the receptive field based on spike rate was normalized by its peak power and is plotted with the ratio power spectrum, as derived in *B* (RF spectrum).

Use of this correction factor for explainable variance in the repeated sequence data had a minimal effect on the variance accounted for by our model predictions, increasing the mean variance accounted for to 43.9% from 38.9%. This modest increase in variance accounted for is expected if the number of trials used for averaging is large, such that the averaging procedure effectively reduces trial-to-trial noise fluctuations (mean number of trials = 16.7). In addition, the modest change in accounted variance may be due to the analog nature of membrane potential relative to spiking. Because there always exists a membrane potential signal, the averaging procedure may be more effective at reducing trial-to-trial fluctuations.

The trial-averaging procedure dramatically increased the quality of our model predictions, increasing the utility of the GP_{SP} in accounting for average membrane potential responses, if not trial-to-trial responses. To examine how averaging altered membrane potential responses, we compared the frequency content of the unaveraged membrane potentials with that of the average membrane potential, and we determined which response frequencies were preserved (Fig. 5*B*). To accurately compare these two frequency spectra across our sample population of neurons, we calculated the ratio of the two frequency spectra and normalized the response ratios (Fig. 5*C*). We found that a band of frequencies between 4 and 10 Hz tended to be preserved after the averaging procedure.

The receptive fields extracted from the noise stimulus were composed of a similar frequency range (4–10 Hz). We extracted the temporal frequency spectrum for each neuron's receptive field by taking the two-dimensional Fourier transform and examining the temporal frequency spectra across spatial frequency. The selective preservation of 4–10 Hz matches the temporal frequency spectrum of the linear receptive fields and explains why the linear model predicted average responses with greater accuracy than trial-to-trial responses (Fig. 5*C*). The averaging procedure retains the frequencies that match those of the linear receptive field while attenuating frequencies that are not directly locked to the stimulus. A significant portion of a neuron's response power lies outside the frequency range of the receptive field (Fig. 5*B*). Although the responses at those frequencies might not be locked to the specific stimulus, they could nonetheless be involved in modulating the neuron's response to the noise sequence (Azouz and Gray 2000; Finn et al. 2007). In summary, using spike rate-derived receptive fields allows a more accurate model of the underlying average membrane potential; averaging responses reduces the trial-to-trial membrane potential variability outside the frequency spectra of the receptive field.

When the relationship between GP_{SP} and mean membrane potential is examined, deviations from a linear relationship are apparent, but only at extreme values of the GP_{SP} (Fig. 4*B*). The biophysical origins of these deviations from linearity may be the result of spike threshold at the high end and the reversal potential for inhibition at the low end of the spectrum. Positive values of GP_{SP} overestimate actual recorded membrane potential depolarizations, whereas negative GP_{SP} values overestimate actual recorded membrane potential hyperpolarizations. One way to correct for this apparent nonlinearity is to pass the output of the linear filter through a sigmoid. To test whether this is appropriate, we fit the relationship between GP_{SP} and the recorded membrane potential [$V(GP)$] using the following sigmoid function:

$$V(\mathrm{GP}) = a\left(\frac{1}{1 + e^{-c(\mathrm{GP}-b)}}\right) \quad (2)$$

where a is the gain of the sigmoid, b is the midpoint of the sigmoid, and c is the steepness of the sigmoid. The sigmoid function provides a slightly better fit of the relationship between GP_{SP} and actual membrane potential than a linear function (39.2% for the sigmoid model vs. 38.9% for the linear model across our sample population of recorded neurons). Although the sigmoid function modestly increases the ability of spike rate to predict membrane potential, it requires use of an additional parameter beyond a simple linear function. To determine whether the increased accuracy of the sigmoid function justifies the additional parameter, we compared the two models using the likelihood-ratio test (Sokal and Rohlf 1969). For none of the neurons in our database did we find that the inclusion of the additional parameter required by the sigmoid was justified ($P > 0.1$, fixed noise sequence data, $n = 13$; $P > 0.1$, variable noise sequence data, $n = 25$). Despite the improved accuracy of the sigmoid fit, the number of data points that exist on the extreme edges of the data is small so that even though the sigmoid function does aid in predicting these values, it does not substantially increase the fit of the model. Thus the relationship between GP_{SP} and recorded membrane

potential in simple cells is better described by a simple linear model.

Threshold as a filter for membrane potential. Simple cell spiking responses deviate significantly from linear expectations, but the underlying basis for the differences between predicted and actual values is unclear. Spiking responses based on noise stimulation systematically underestimate spiking selectivity for orientation tuning (Gardner et al. 1999), spatial and temporal frequency (DeAngelis et al. 1993b), direction (Albrecht and Geisler 1991; DeAngelis et al. 1993b; Reid et al. 1987, 1991), and binocular disparity (Anzai et al. 1999). As in previous reports, we found that our expectation of response (GP_{SP}), derived from the spiking responses to the noise stimulus, is related to recorded spike rate in a nonlinear fashion (Fig. 4*C*). Negative values of GP_{SP} are associated with zero or very low spike rates, and spike rate increases in an expansive fashion with increasing GP_{SP}. It has been hypothesized that a simple threshold may account for this nonlinear relationship. If so, then the relationship between GP_{SP} and recorded spike rate, a relationship constructed solely based on spike rate responses, should match the relationship between recorded membrane potential and spike rate.

Importantly, we also observed a nonlinear relationship between recorded membrane potential and spike rate (Carandini and Ferster 2000; Finn et al. 2007; Priebe and Ferster 2005, 2006; Sanchez-Vives et al. 2000). To compare these GP_{SP}-spike rate and membrane potential-spike rate relationships, we first measured the distributions of the recorded membrane potential (Fig. 6*A*), the GP_{SP} (Fig. 6*B*), and the recorded spike rate (Fig. 6*C*). The transformation between GP_{SP} and spike rate (Fig. 6*B*, *inset*) displays the same expansive nonlinearity as that observed between the actual membrane potential and spike rate (Fig. 6*A*, *inset*). To quantify the degree of correspondence between these transformations, we overlaid the recorded membrane potential-to-spike rate transformation and the GP_{SP}-to-spike rate transformation (Fig. 6*E*, for 3 neurons). Note that this comparison may only be done for conditions in which we have recorded the membrane potential responses to a fixed noise stimulus, since with a fixed noise stimulus we have an accurate estimate of the mean and standard deviation of the membrane potential, which should be related to GP_{SP}. For each of the 13 neurons in our sample population that was presented the fixed noise stimulus, these nonlinear functions overlapped one another (mean $R^2 = 0.84$), indicating that measures of the nonlinear transformation of GP_{SP} to recorded spike rate reflect the actual nonlinear transformation from membrane potential to spike rate and are not consequences of factors such as shunting inhibition that occur before integration of synaptic inputs into membrane potential.

One result of spike threshold is the separation of stimulus conditions that elicit small membrane potential deviations from stimulus conditions that elicit large membrane potential deviations. Because membrane potential must reach a threshold potential in order for the neuron to generate an action potential, the distribution of spike rate and membrane potential response should be different (Carandini 2004). The distribution of membrane potential responses to our noise stimulus is roughly Gaussian (Fig. 6*A*), but the distribution of spiking responses is skewed and has a long tail (Fig. 6*C*). This change in response statistics can be encapsulated by the skew and kurtosis of the distributions (the third and fourth moments) (Ringach and Malone 2007). For the example neuron in Fig. 6, the observed spike rate skew (1.39) was higher than the skew found in membrane potential and GP_{SP} distributions (0.24 and −0.08, respectively). Furthermore, the observed spike rate kurtosis was also higher for spike rate (9.64) than the kurtosis found in membrane potential and GP_{SP} distributions (2.31 and 3.56, respectively). These increases in skew and kurtosis observed in the example neuron in Fig. 6 reflect changes that we observed across our entire sample population of neurons (see Table 1).

This change in response skew and kurtosis could be a simple consequence of the spike threshold's filtering of the

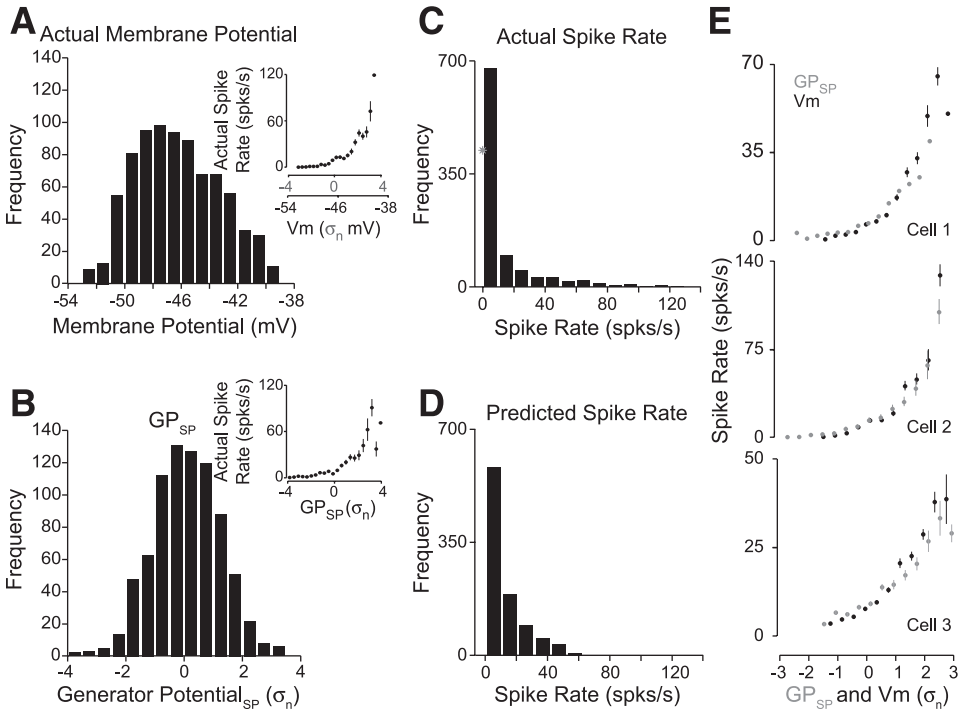

Fig. 6. Comparison of threshold nonlinearities. *A*: distribution of recorded membrane potential responses to a noise stimulus. *Inset* shows the relationship between average membrane potential and spike rate. *B*: distribution of GP_{SP}. *Inset* shows the relationship between GP_{SP} and recorded spike rate. *C*: distribution of spike rate in response to the noise stimulus. Asterisk indicates the number of bins with no spike rate. *D*: predicted distribution of spike rate given by passing GP_{SP} through the threshold nonlinearity. *E*: relationship between GP_{SP} and spike rate (gray symbols) is plotted with the relationship between average membrane potential and spike rate (black symbols) for 3 example neurons.

Table 1. *Summary of response statistics*

	Skew	Kurtosis
V_m	0.59 ± 0.49	3.21 ± 0.74
Spike rate	2.11 ± 0.88	14.18 ± 6.50
GP_{SP}	0.01 ± 0.14	2.77 ± 0.89
Predicted spike rate	1.24 ± 0.71	4.80 ± 2.59

Values are means ± SD across the sample population of recorded neurons. Vm, membrane potential; GP_{SP}, generator potential based on spiking.

neuron's inputs. To determine whether the threshold nonlinearity could account for these changes, we applied a threshold to the observed membrane potential to create a predicted spike rate (Fig. 6*D*). A variety of different functions have been used to characterize this relationship, including threshold-linear, power-law, or more complex functions (Carandini and Ferster 2000; Hansel and van Vreeswijk 2002; Miller and Troyer 2002); for simplicity, we have used a threshold-linear relationship:

$$R(V_m) = a\lfloor V_m - V_{th} \rfloor_+^p \quad (3)$$

where V_m is the membrane potential, V_{th} is the threshold potential, a is the gain of the response beyond the critical threshold potential, + indicates the Heaviside function, p is an exponent nonlinearity (set to 1 for a threshold-linear fit), and membrane potential is expressed in units of the standard deviation. An increase in the skew of the response distribution is predicted by the simple nonlinear threshold transformation (Fig. 6*D*, skew = 2.52), but the predicted increase generally underestimates the change in distribution of the skew. In the same way, the kurtosis of the predicted spike rate (4.29) is larger than that of the actual recorded membrane potential (2.31) but also underestimates the kurtosis observed in the actual recorded spike rate (9.64). Overall, the changes in response statistics predicted by a simple threshold-linear model are in the right direction but underestimate the actual increases in skew and in kurtosis observed between membrane potential and spike rate (Table 1). Replacing the threshold-linear model with a power-law model, by allowing p to vary while fixing V_{th} to the resting potential in *Eq. 3*, had negligible effects on increases in skew and kurtosis. Although it may be that more sophisticated models for threshold could account for the residual changes in skew and kurtosis, our data demonstrate that simple threshold models applied to membrane potential will increase skew and kurtosis as observed in our actual data.

DISCUSSION

Extracellular records, generated with either electrophysiological or imaging techniques, have become the dominant measure of sensory selectivity in the cerebral cortex. Such recordings describe the information a neuron communicates to downstream targets via spikes, but they generally provide a distorted representation of the synaptic inputs to the neuron that lead to its spiking response. Many reports now exist that demonstrate substantial differences between the selectivity of a neuron's input and its output (Carandini and Ferster 2000; Escabi et al. 2005; Moore and Nelson 1998; Nowak et al. 2010; Priebe et al. 2004; Tan et al. 2004). One of the major contributors to this distortion is the presence of the neuron's threshold nonlinearity (Mechler and Ringach 2002; Priebe and Ferster 2008).

From electrophysiological records of membrane potential, one can estimate accurately a neuron's average spike rate by applying a threshold nonlinearity (Carandini and Ferster 2000; Finn et al. 2007; Priebe and Ferster 2005, 2006; Sanchez-Vives et al. 2000). In this study we have asked the converse question: can we estimate membrane potential, and therefore, a neuron's synaptic input, on the basis of spike rate records alone? One method that may reveal the underlying membrane potential from a neuron's spike rate is to generate linear receptive field estimates and use those estimates to predict membrane potential. If membrane potential and spike rate are separated by a single static nonlinearity, it should be possible to predict membrane potential from spike rate. We have tested this hypothesis for the first time by directly comparing models based on spike rate with membrane potential responses. Using a commonly employed dynamic noise stimulus, we have demonstrated that linear receptive fields extracted from membrane potential and spike rate are virtually identical. The correspondence of the linear receptive fields in this case is expected despite the presence of a threshold nonlinearity, as long as the threshold nonlinearity is static (Bussgang 1952; de Boer and Kuyper 1968). This correspondence of the receptive field also suggested that predictions of membrane potential from spike rate should be possible.

Although we found a precise correspondence of membrane potential and spike rate linear receptive fields, predictions of membrane potential from spike rate (spiking generator potential, GP_{SP}) accounted for only 15–20% of the actual membrane potential response we recorded on a trial-to-trial basis. We hypothesize that there are at least three effects that may be reducing the quality of the linear model. First, ongoing activity within the "resting" cortex suggests that the neuron's initial condition for each stimulus presentation varies and that the ongoing activity adds a component of neural "noise" into the trial-to-trial membrane potential variability. This trial-to-trial variability cannot be accounted for using our simple model. Attempting to reduce the trial-to-trial membrane potential variability, we averaged membrane potential responses across trials, which significantly increased the ability of our simple model to predict membrane potential. The predictions from our simple model based on spike rate accounted for ~45% of the average membrane potential responses. Increasing the number of trials used to create the average response may further reduce the membrane potential variability. Use of a method to account for the impacts of our finite validation data set on explainable variable, however, did not dramatically increase estimates of the predictive power of the linear model (Machens et al. 2004; Sahani and Linden 2003). Second, the underlying membrane potential response could contain nonlinear components that we cannot account for using a linear model. To reduce the effects of the known nonlinearities in V1, we restricted our analysis to cortical neurons that were classified as simple cells by the F1/F0 modulation ratio, and we excluded highly nonlinear complex cells. Despite this selection, even simple cells contained nonlinear components in their responses (Priebe et al. 2004). An alternative method that includes multiple filters and nonlinear transformations may help to account for a higher degree of membrane potential variance (Rust et al. 2005; Touryan et al. 2002). Third, the act of firing an action potential

causes a distortion of the neuronal membrane potential that cannot be captured using the simple linear receptive field estimates employed here (Pillow et al. 2005). The membrane potential traces we used to fit our data originally contained spikes that were filtered out with a median filter. Median filtering removes the large brief deviations characteristic of spikes, but any effect that the spike had on the subsequent membrane potential, such as afterhyperpolarizations, cannot be accounted for with our spike rate-based model.

Although it is important to note these possible confounding factors relevant to our simple model, our model's predictions of membrane potential from spike rate are nonetheless very similar to those produced by linear models based on membrane potential itself (mean $R^2 = 0.8$, between GP_{VM} and GP_{SP}). It appears, therefore, that the spike rate-based model can do just as well as a linear model for estimating underlying membrane potential, and the failure of the receptive field model is not due to a lack of sufficient spiking data, but instead one or more of the three possible effects detailed above.

Comparisons of membrane potential selectivity and spike rate selectivity in V1 neurons generally demonstrate broader tuning for membrane potential than spike rate (Bringuier et al. 1999; Priebe and Ferster 2008). From extracellular recordings in V1, predictions of orientation and direction selectivity on the basis of linear receptive fields generally underestimate the degree of selectivity exhibited in response to bars or gratings (DeAngelis et al. 1993a, 1993b; Gardner et al. 1999). Here, for the first time, we are able to link these two findings, demonstrating that the spike rate spatiotemporal selectivity of simple cells extracted from the noise stimulus is directly related to the membrane potential spatiotemporal selectivity. We found that predictions based on spike rate in response to the noise stimulus are directly related to membrane potential selectivity, and thus underestimate selectivity to simple grating stimuli. It is important to recognize that the statistics of these stimulus regimes are different, and those statistics have consequences for the estimate of the stimulus selectivity (see also Fournier et al. 2011). In addition, we have demonstrated that the same expansive nonlinearity used to relate GP_{SP} to actual spike rate (Fig. 6) may be applied to transform recorded membrane potential to spike rate. This match between nonlinear transformations strongly suggests that the threshold nonlinearity accounts for the expansive nonlinear response described extensively along the visual pathway (Anzai et al. 1999; Bonin et al. 2006; Chander and Chichilnisky 2001; Sharpee et al. 2006).

A central outcome of our analysis is that the same receptive fields emerge from recordings of spike rate and membrane potential, a finding that requires the intervening threshold nonlinearity to be static. The threshold nonlinearity displayed here appears to be based on two components: the neuron's biophysical spike threshold and its membrane potential variability (Anderson et al. 2000; Hansel and van Vreeswijk 2002; Miller and Troyer 2002; Priebe and Ferster 2008). If either component were to change, threshold would no longer be static and our analysis would no longer be valid. Whereas the biophysical spike threshold is unlikely to change, the level of background membrane potential variability can change dramatically in neurons of visual cortex (Azouz and Gray 1999). Trial-to-trial membrane potential variability will change with changes in stimulus contrast such that high-contrast stimuli reduce overall membrane potential variability (Finn et al. 2007). Because stimulus contrast alters the shape of the threshold nonlinearity, leading to an increased gain between membrane potential and spike rate for low contrasts, using stimuli composed of different contrasts may reveal discrepancies between membrane potential and spike rate selectivity that are not apparent in the fixed contrast stimuli we have employed.

Our goals with this study were *1*) to determine whether membrane potential, recognized to be representative of the neuron's synaptic inputs, can be predicted on the basis of recorded spike rate alone and *2*) to understand the biophysical basis for the nonlinear transformation that emerges from the receptive field analysis. Our hypothesis was that generator potential estimates based on spike rate should match recorded membrane potential. Our results support this idea, although the predictive power of the linear model was only ~45%. The membrane potential response frequency spectrum was much broader than the receptive field frequency spectrum, allowing the model to account for only a minority of the membrane potential variance (Fig. 5). Membrane potential responses contain power in both the alpha band range (<2 Hz) as well as the higher frequency range that is not predicted from the linear receptive field. Our analysis has provided a clear interpretation of the output nonlinearity that appears between modeled GP_{SP} and recorded spike rate as well as between recorded membrane potential and recorded spike rate. Because these two relationships are tightly coupled, this expansive nonlinearity reflects a process that occurs after the integration of excitatory and inhibitory inputs.

We employed a dynamic noise stimulus because of its long history of use in studying response properties of visual cortical neurons and because its properties allow for a simple estimation of spike rate and membrane potential receptive fields. It should nonetheless be possible to employ a range of different stimuli to uncover the underlying membrane potential receptive field structure from spike rate. For example, natural scenes may also be used to estimate the underlying receptive fields of sensory neurons, although statistical corrections may need to be made due to distortions in the tiling of stimulus space (Sharpee et al. 2008). The use of more sophisticated methods to reconstruct feature selectivity, including the use of methods that extract multiple filters, may increase the degree to which spike rate can predict membrane potential fluctuations, even for cortical simple cells that are generally characterized by a single filter (Brenner et al. 2000; Rust et al. 2005; Sharpee 2007). In addition, it should be possible to use spike timing to improve predictions of membrane potential. Spikes directly influence membrane potential fluctuations by resetting the membrane potential and by altering the composition of the open conductances (Badel et al. 2008; Pillow et al. 2005, 2008). It is also possible to take advantage of the timing of spikes to make constraints on the intervening membrane potential fluctuations (Koyama and Paninski 2010; Paninski 2006). Thus taking spike timing into consideration could improve the predictive power of extracellular records in inferring the underlying membrane potential.

In summary, we have demonstrated the utility of using spike-based estimates of membrane potential, but we have also revealed the limitations of this approach. It is possible to reconstruct average membrane potential responses solely from spike rate responses using a commonly employed noise stimulus, providing access to the underlying membrane potential

selectivity on the basis of spike rate alone in V1 simple cells. With the use of this straightforward method, which requires only spiking records, it is possible to characterize the basis of response selectivity at the level of the aggregate synaptic input and thus place important constraints on the functional organization of cortex.

ACKNOWLEDGMENTS

We are grateful to Jessica Hanover, Andrew Tan, David Ferster, Jonathan Pillow, and Evan Archer for helpful discussions.

GRANTS

This work was supported by National Eye Institute Grant EY-019288 and the Pew Charitable Trusts.

DISCLOSURES

No conflicts of interest, financial or otherwise, are declared by the author(s).

AUTHOR CONTRIBUTIONS

Author contributions: D.M. and N.J.P. analyzed data; D.M. and N.J.P. interpreted results of experiments; D.M. and N.J.P. prepared figures; D.M. and N.J.P. drafted manuscript; D.M. and N.J.P. edited and revised manuscript; D.M., B.S., and N.J.P. approved final version of manuscript; B.S. and N.J.P. performed experiments; N.J.P. conception and design of research.

REFERENCES

Albrecht DG, Geisler WS. Motion selectivity and the contrast-response function of simple cells in the visual cortex. *Vis Neurosci* 7: 531–546, 1991.

Anderson JS, Lampl L, Gillespie D, Ferster D. The contribution of noise to contrast invariance of orientation tuning in cat visual cortex. *Science* 290: 1968–1971, 2000.

Anzai A, Ohzawa I, Freeman RD. Neural mechanisms for processing binocular information. I. Simple cells. *J Neurophysiol* 82: 891–908, 1999.

Azouz R, Gray CM. Cellular mechanisms contributing to response variability of cortical neurons in vivo. *J Neurosci* 19: 2209–2223, 1999.

Azouz R, Gray CM. Dynamic spike threshold reveals a mechanism for synaptic coincidence detection in cortical neurons in vivo. *Proc Natl Acad Sci USA* 97: 8110–8115, 2000.

Badel L, Lefort S, Brette R, Petersen CC, Gerstner W, Richardson MJ. Dynamic *I-V* curves are reliable predictors of naturalistic pyramidal-neuron voltage traces. *J Neurophysiol* 99: 656–666, 2008.

Bonin V, Mante V, Carandini M. The statistical computation underlying contrast gain control. *J Neurosci* 26: 6346–6353, 2006.

Brainard DH. The Psychophysics Toolbox. *Spat Vis* 10: 443–446, 1997.

Brenner N, Bialek W, de Ruyter van Steveninck R. Adaptive rescaling maximizes information transmission. *Neuron* 26: 695–702, 2000.

Bringuier V, Chavane F, Glaeser L, Fregnac Y. Horizontal propagation of visual activity in the synaptic integration field of area 17 neurons. *Science* 283: 695–699, 1999.

Bussgang JJ. *Crosscorrelation Functions of Amplitude-Distorted Gaussian Signals*. Cambridge, MA: Research Laboratory of Electronics, Massachusetts Institute of Technology, 1952, p. 14.

Carandini M. Amplification of trial-to-trial response variability by neurons in visual cortex. *PLoS Biol* 2: e264, 2004.

Carandini M, Ferster D. Membrane potential and firing rate in cat primary visual cortex. *J Neurosci* 20: 470–484, 2000.

Chander D, Chichilnisky EJ. Adaptation to temporal contrast in primate and salamander retina. *J Neurosci* 21: 9904–9916, 2001.

Chichilnisky EJ. A simple white noise analysis of neuronal light responses. *Network* 12: 199–213, 2001.

Citron MC, Emerson RC. White noise analysis of cortical directional selectivity in cat. *Brain Res* 279: 271–277, 1983.

Dayan P, Abbott LF. *Theoretical Neuroscience: Computational and Mathematical Modeling of Neural Systems*. Cambridge, MA: MIT Press, 2001.

de Boer R, Kuyper P. Triggered correlation. *IEEE Trans Biomed Eng* 15: 169–179, 1968.

DeAngelis GC, Ohzawa I, Freeman RD. Spatiotemporal organization of simple-cell receptive fields in the cat's striate cortex. I. General characteristics and postnatal development. *J Neurophysiol* 69: 1091–1117, 1993a.

DeAngelis GC, Ohzawa I, Freeman RD. Spatiotemporal organization of simple-cell receptive fields in the cat's striate cortex. II. Linearity of temporal and spatial summation. *J Neurophysiol* 69: 1118–1135, 1993b.

Escabi MA, Nassiri R, Miller LM, Schreiner CE, Read HL. The contribution of spike threshold to acoustic feature selectivity, spike information content, and information throughput. *J Neurosci* 25: 9524–9534, 2005.

Finn IM, Priebe NJ, Ferster D. The emergence of contrast-invariant orientation tuning in simple cells of cat visual cortex. *Neuron* 54: 137–152, 2007.

Fournier J, Monier C, Pananceau M, Fregnac Y. Adaptation of the simple or complex nature of V1 receptive fields to visual statistics. *Nat Neurosci* 14: 1053–1060, 2011.

Gardner JL, Anzai A, Ohzawa I, Freeman RD. Linear and nonlinear contributions to orientation tuning of simple cells in the cat's striate cortex. *Vis Neurosci* 16: 1115–1121, 1999.

Hansel D, van Vreeswijk C. How noise contributes to contrast invariance of orientation tuning in cat visual cortex. *J Neurosci* 22: 5118–5128, 2002.

Hirsch JA, Alonso JM, Reid RC, Martinez LM. Synaptic integration in striate cortical simple cells. *J Neurosci* 18: 9517–9528, 1998.

Hubel DH, Wiesel TN. Receptive fields, binocular interaction and functional architecture in the cat's visual cortex. *J Physiol* 160: 106–154, 1962.

Jagadeesh B, Wheat HS, Kontsevich L, Tyler CW, Ferster D. Direction selectivity of synaptic potentials in simple cells of the cat visual cortex. *J Neurophysiol* 78: 2772–2789, 1997.

Koyama S, Paninski L. Efficient computation of the maximum a posteriori path and parameter estimation in integrate-and-fire and more general state-space models. *J Comput Neurosci* 29: 89–105, 2010.

Machens CK, Wehr MS, Zador AM. Linearity of cortical receptive fields measured with natural sounds. *J Neurosci* 24: 1089–1100, 2004.

Mclean J, Palmer LA. Contribution of linear mechanisms to direction selectivity of simple cells in area 17 and 18 of the cat. *Invest Ophthalmol Visual Sci* 29, *Suppl*: 23, 1988.

Mechler F, Ringach DL. On the classification of simple and complex cells. *Vision Res* 42: 1017–1033, 2002.

Miller KD, Troyer TW. Neural noise can explain expansive, power-law nonlinearities in neural response functions. *J Neurophysiol* 87: 653–659, 2002.

Monier C, Chavane F, Baudot P, Graham LJ, Fregnac Y. Orientation and direction selectivity of synaptic inputs in visual cortical neurons: a diversity of combinations produces spike tuning. *Neuron* 37: 663–680, 2003.

Moore CI, Nelson SB. Spatio-temporal subthreshold receptive fields in the vibrissa representation of rat primary somatosensory cortex. *J Neurophysiol* 80: 2882–2892, 1998.

Nowak LG, Sanchez-Vives MV, McCormick DA. Spatial and temporal features of synaptic to discharge receptive field transformation in cat area 17. *J Neurophysiol* 103: 677–697, 2010.

Paninski L. The most likely voltage path and large deviations approximations for integrate-and-fire neurons. *J Comput Neurosci* 21: 71–87, 2006.

Pelli DG. The VideoToolbox software for visual psychophysics: transforming numbers into movies. *Spat Vis* 10: 437–442, 1997.

Pillow JW, Paninski L, Uzzell VJ, Simoncelli EP, Chichilnisky EJ. Prediction and decoding of retinal ganglion cell responses with a probabilistic spiking model. *J Neurosci* 25: 11003–11013, 2005.

Pillow JW, Shlens J, Paninski L, Sher A, Litke AM, Chichilnisky EJ, Simoncelli EP. Spatio-temporal correlations and visual signalling in a complete neuronal population. *Nature* 454: 995–999, 2008.

Priebe NJ, Ferster D. Direction selectivity of excitation and inhibition in simple cells of the cat primary visual cortex. *Neuron* 45: 133–145, 2005.

Priebe NJ, Ferster D. Inhibition, spike threshold, and stimulus selectivity in primary visual cortex. *Neuron* 57: 482–497, 2008.

Priebe NJ, Ferster D. Mechanisms underlying cross-orientation suppression in cat visual cortex. *Nat Neurosci* 9: 552–561, 2006.

Priebe NJ, Mechler F, Carandini M, Ferster D. The contribution of spike threshold to the dichotomy of cortical simple and complex cells. *Nat Neurosci* 7: 1113–1122, 2004.

Reid RC, Soodak RE, Shapley RM. Directional selectivity and spatiotemporal structure of receptive fields of simple cells in cat striate cortex. *J Neurophysiol* 66: 505–529, 1991.

Reid RC, Soodak RE, Shapley RM. Linear mechanisms of directional selectivity in simple cells of cat striate cortex. *Proc Natl Acad Sci USA* 84: 8740–8744, 1987.

Rieke F, Warland D, de Ruyter van Steveninck RR, Bialek W. *Spikes: Exploring the Neural Code*. Cambridge, MA: MIT Press, 1997.

Ringach DL, Malone BJ. The operating point of the cortex: neurons as large deviation detectors. *J Neurosci* 27: 7673–7683, 2007.

Rust NC, Schwartz O, Movshon JA, Simoncelli EP. Spatiotemporal elements of macaque V1 receptive fields. *Neuron* 46: 945–956, 2005.

Sahani M, Linden JF. How Linear are Auditory Cortical Responses? *Adv Neural Inform Proc Syst* 125–132, 2003.

Sanchez-Vives MV, Nowak LG, McCormick DA. Membrane mechanisms underlying contrast adaptation in cat area 17 in vivo. *J Neurosci* 20: 4267–4285, 2000.

Sharpee TO. Comparison of information and variance maximization strategies for characterizing neural feature selectivity. *Stat Med* 26: 4009–4031, 2007.

Sharpee TO, Miller KD, Stryker MP. On the importance of static nonlinearity in estimating spatiotemporal neural filters with natural stimuli. *J Neurophysiol* 99: 2496–2509, 2008.

Sharpee TO, Sugihara H, Kurgansky AV, Rebrik SP, Stryker MP, Miller KD. Adaptive filtering enhances information transmission in visual cortex. *Nature* 439: 936–942, 2006.

Simoncelli EP, Pillow JW, Paninski L, Schwartz O. Characterization of neural response with stochastic stimuli. In: *The Cognitive Neurosciences* (3rd ed.), edited by Gazzaniga M. Cambridge, MA: MIT Press, 2004, p. 327–338.

Skottun BC, De Valois RL, Grosof DH, Movshon JA, Albrecht DG, Bonds AB. Classifying simple and complex cells on the basis of response modulation. *Vision Res* 31: 1079–1086, 1991.

Sokal RR, Rohlf FJ. *Biometry: the Principles and Practice of Statistics in Biological Research*. San Francisco: Freeman, 1969, p. xxi.

Tan AY, Zhang LI, Merzenich MM, Schreiner CE. Tone-evoked excitatory and inhibitory synaptic conductances of primary auditory cortex neurons. *J Neurophysiol* 92: 630–643, 2004.

Touryan J, Lau B, Dan Y. Isolation of relevant visual features from random stimuli for cortical complex cells. *J Neurosci* 22: 10811–10818, 2002.